Letter | Editors' Suggestion

Evidence for giant surface Dzyaloshinskii-Moriya interaction in the chiral magnetic insulator Cu_2OSeO_3

Wancong Tan,[1,*] Haonan Jin,[1,2,*] Raymond Fan,[3] Kejing Ran,[1,2,4,†] and Shilei Zhang[1,2,5,‡]

[1]*School of Physical Science and Technology, ShanghaiTech University, Shanghai 200031, China*

[2]*ShanghaiTech Laboratory for Topological Physics, ShanghaiTech University, Shanghai 200031, China*

[3]*Diamond Light Source, Didcot, OX11 0DE, United Kingdom*

[4]*College of Physics & Center of Quantum Materials and Devices, Chongqing University, Chongqing 401331, China*

[5]*Center for Transformative Science, ShanghaiTech University, Shanghai 200031, China*

(Received 15 November 2023; accepted 17 May 2024; published 5 June 2024)

Broken of translational symmetry plays a vital role in the stabilization of three-dimensional magnetic skyrmions. The absence of exchange neighbours at truncated surfaces leads to surface twist effect, resulting in twisted helicity angle of the skyrmions. Recently, it was reported in Zhang *et al.* [Proc. Natl. Acad. Sci. USA **115**, 6386 (2018)] that the observed surface twist effect is over an order of magnitude more pronounced than the theoretical predictions. Nevertheless, the underlying mechanism that leads to such discrepancy has not been resolved yet. In order to address this long-standing issue, we performed depth-resolved circular dichroic resonant elastic x-ray scattering (CD-REXS) measurements on the skyrmion lattice phase in Cu_2OSeO_3 over a wide temperature range. It is found that the measured skyrmion helicity angle profile is highly temperature-dependent, which cannot be quantitatively explained by the temperature-varying micromagnetic parameters alone. By systematically ruling out other possible effects, we conclude that a giant surface-type Dzyaloshinskii-Moriya interaction emerges due to the ferroelectric polarization at the surface of Cu_2OSeO_3. Our results provide insights into the complex interplay between surface and bulk interactions in the formation of magnetic skyrmions and offer new possibilities for designing skyrmionic devices.

DOI: 10.1103/PhysRevB.109.L220402

Magnetic skyrmions are topologically protected spin textures with particlelike properties [1,2]. Their topological structures give rise to novel magnetoelectric transport effects [3–8] and nontrivial spin dynamics [9–11], establishing the modern concept of emergent electromagnetism [12]. Moreover, their structural robustness and manipulation easiness have facilitated the development of innovative concepts for spintronic devices [4,6,13,14]. Therefore exploring novel skyrmion formation mechanism is of crucial importance for both advanced material research in magnetism and cutting-edge information technology.

Skyrmion formation is usually observed in materials that are in lack of inversion symmetry, from which antisymmetric exchange interaction, Dzyaloshinskii-Moriya interaction (DMI), results [2,15,16]. The winding fashion of a skyrmion is intrinsically determined by the type of the DMI from the material, called the *helicity angle* χ [17]. For example, Bloch-type skyrmions with $\chi = \pm 90^\circ$ can be stabilized in chiral magnets, which host the bulk-type DMI [16,18]. On the other hand, Néel-type skyrmions with $\chi = 0^\circ$ or 180° exist in artificially synthesised ferromagnetic thin films with interfacial DMI [6,19].

Recently, it was recognized that extrinsic mechanisms can further modify the helicity angle of a skyrmion [17,20–26]. For instance, the lack of the translational symmetry at the very surface of a chiral magnet leads to the *surface twist* effect [17,20–22]. As consequence, a distinctive 3D skyrmion structure that is normal to the truncated surface is formed, characterized by a depth-dependent $\chi(z)$ profile [20,27], reads

$$\chi(z) = (\chi_0 - 90^\circ)e^{-z/L_p} + 90^\circ, \tag{1}$$

where χ_0 is the helicity angle of the very top surface, L_p measures the penetration depth of the surface twist effect. Recently, such effect has been experimentally observed in chiral magnets, not only thin plate form [22], but also at the surface of bulk material [17,20,28].

Nonetheless, a quantitative agreement between the experimental observations and the theoretical predictions for such surface twist effect has never been reached. In a recent study in helimagnet Cu_2OSeO_3, a depth-dependent $\chi(z)$ measurement was performed for the skyrmion lattice phase at a fixed temperature [17,20]. The extracted χ_0 measures 180°, which is much larger than the theoretical value of 135° from the standard surface twist model [20]. Moreover, the penetration length of the twist L_p measures 62.5 nm, which is over an order of magnitude larger than the predicted depth of 6 nm [20]. Such large discrepancy indicates the existence of exotic energetics being responsible, whereas remaining elusive so far.

Here, we revisit such long-standing issue by performing depth-resolved $\chi(z)$ measurements in Cu_2OSeO_3. Cu_2OSeO_3 is an insulating chiral magnet that hosts 3D skyrmion lattice

*These authors contributed equally to this work.

†rankj@shanghaitech.edu.cn

‡shilei.zhang@shanghaitech.edu.cn

phase (SkX) [29,30]. Typically, the SkX phase is confined to a limited temperature window (less than 2 K) within the phase diagram, nearby the ordering transition temperature $T_C \sim 58$ K, and enclosed by two critical fields H_{C1} and H_{C2}. The upper limit H_{C2} is around 37 mT, while the lower bound H_{C1} is around 17 mT for the field along the [001] direction [30,31]. Using the fast field-cooling (FC) protocol, the SkX can be metastably extended over a broader temperature range [26,32,33], enabling us to readily examine the temperature dependence of the twist effect.

A single crystal of Cu_2OSeO_3 with a (001) orientation was utilized in this study, prepared through the chemical-vapor-transport method as detailed in Ref. [25]. The high crystalline quality and single-chirality were confirmed using x-ray single crystal diffraction with Cu K_α radiation.

Characterizationwise, we employ depth-dependent circular dichroic resonant elastic x-ray scattering (CD-REXS) technique to retrieve the $\chi(z)$ information [25,26,34]. Combined with our newly developed iterative reconstruction algorithm, the exact $\chi(z)$ profile can be unambiguously reconstructed, instead of being fitted in [20,25]. For a 2D skyrmion texture, the circular dichroism (CD) amplitude I_{2D} is written as

$$I_{2D}(\Psi) = Y \sin(\Psi + \chi), \tag{2}$$

where Ψ is the azimuthal angle of the magnetic satellites spanning within the q_x-q_y plane, and Y is a constant that is governed by the scattering geometry [25,35]. A typical CD-REXS pattern can be found in Fig. 1(a), from which a dichroism extinction vector that divides the positive and negative parts of the CD signal can be identified. The condition $I = 0$ indicates that the extinction condition has been reached. According to Eq. (2), $\sin(\Psi + \chi) = 0$, then $\chi = -\Psi_{ext}$ or $180^\circ - \Psi_{ext}$, where Ψ_{ext} is Ψ angle of the extinction vector. Therefore the Ψ angle of the extinction vector uniquely reveals χ in a 2D case.

For the scenario of a 3D skyrmion system that presents well-defined $\chi(z)$ profile, the experimentally measured I_m is an average value over all layers, which is a function of both Ψ and the photon energy $\hbar\omega$:

$$I_m(\Psi, \hbar\omega) = \sqrt{A^2 + B^2}\sin(\Psi + \chi_m), \tag{3}$$

where

$$A = Y \sum_0^\infty b(z)\cos[\chi(z)], \tag{4}$$

$$B = Y \sum_0^\infty b(z)\sin[\chi(z)], \tag{5}$$

$$b(z) = e^{z\sec\alpha/\Lambda(\hbar\omega)}/\Lambda(\hbar\omega), \tag{6}$$

$$\chi_m = \arctan(B/A), \tag{7}$$

where α is the x-ray incidence angle, Λ is the x-ray penetration length that is quantitatively known [20].

First, it is clear that an extinction vector can be experimentally identified in a similar way as that of the 2D case. This leads to a well-defined χ_m, as illustrated in Figs. 1(a)–1(d). More importantly, as suggested by Eq. (7), the measured χ_m is photon energy dependent, which is an averaged helicity angle that contains the information of $\chi(z)$. Therefore a χ_m scan over $\hbar\omega$ contains the full knowledge of $\chi(z)$. This forms the basics of our iterative reconstruction algorithm that can retrieve the exact 3D profile of the helicity angle.

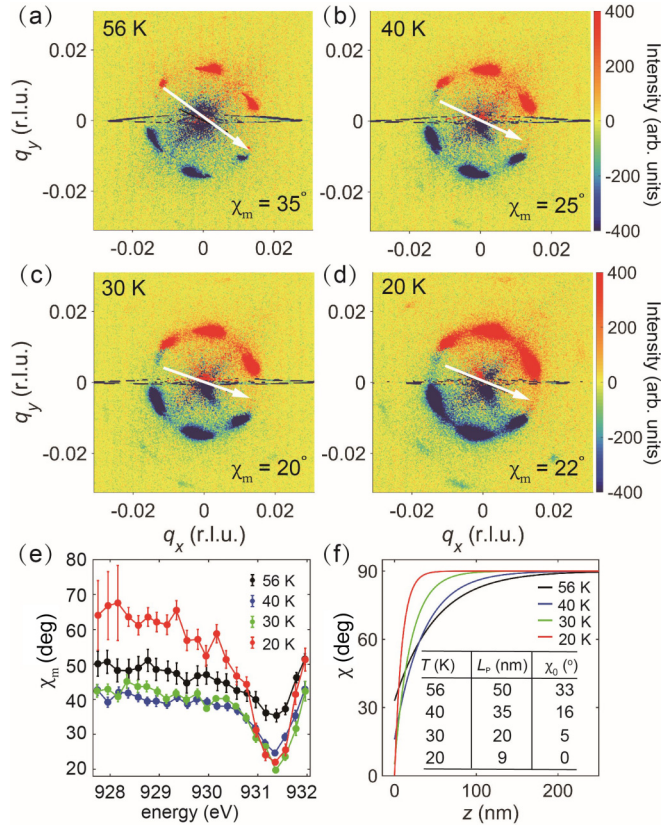

FIG. 1. [(a)–(d)] CD-REXS patterns measured at different temperatures under 35 mT, using photon energy of 931.25 eV at Cu L_3 edge. The orientation of the extinction vector is marked by the white arrows. Their azimuthal angles Ψ directly reveal the measured helicity angles χ_m. (e) χ_m as a function of photon energy at various temperatures. The lines represents the best fit to the experimental data points (dots), yielding the depth dependence of χ shown in (f). (f) The reconstructed $\chi(z)$ profiles at different temperatures, obtained from (e). The inset table lists the extracted χ_0 and L_p values.

We first perform the CD-REXS mappings at fixed photon energy of 931.25 eV, i.e., at the Cu L_3 edge. A fixed 35 mT external field $B \parallel [001]$ is applied along the z direction, in order to stabilize the SkX phase. The CD intensity is the subtraction of the intensities measured with left- and right-circularly polarized incident x-rays. As shown in the figures, the distinct pattern of a hexagonal SkX featuring six magnetic Bragg peaks within the q_x-q_y plane. The extinction vectors are marked with white arrows in Figs. 1(a)–1(d), from which χ_m can determined to be 35° at $T = 56$ K, 25° at 40 K, 20° at 30 K, and 22° at 20 K, respectively. Such strong temperature dependence of χ_m has not been observed nor reported before, indicating the temperature-varying 3D $\chi(z)$ profile.

We thus perform an energy scan of the measured average helicity angle $\chi_m(\hbar\omega)$, from which the exact $\chi(z)$ curve can be obtained. Figure 1(e) shows the experimentally measured "spectra" of χ_m at different temperatures. Our iterative reconstruction method from Fig. 1(e) leads to the depth-resolved helicity angle evolution $\chi(z)$, as shown in Fig. 1(f). First, it

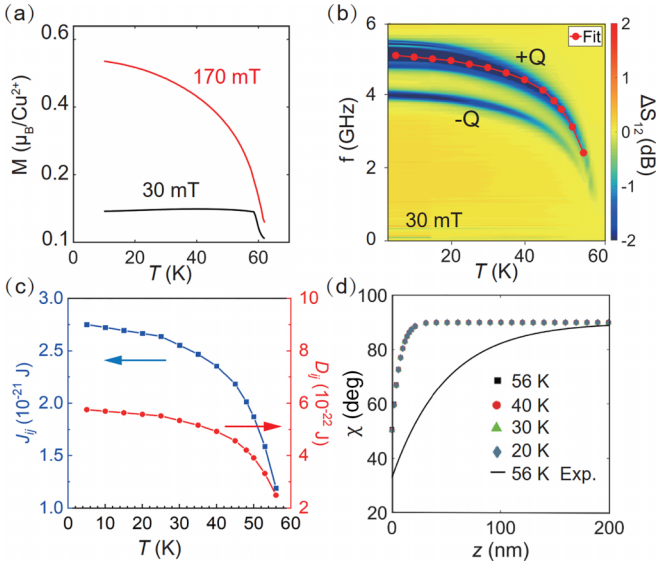

FIG. 2. (a) Temperature dependence of the magnetization of Cu_2OSeO_3 single crystal under 30 mT and 170 mT measured by SQUID. (b) Microwave absorption spectra of Cu_2OSeO_3 at 30 mT. Data was recorded under temperatures from 3 to 62 K with step size of 1 K. The colormap encodes the transmission difference ΔS_{12}. Data at 62 K are subtracted as background. The red dotted line marks the fit to $+Q$ mode by micromagnetic simulation. The corresponding fitted exchange parameters D_{ij} and J_{ij} are plotted in (c). (d) Simulated $\chi(z)$ at various temperatures using the parameters shown in (c), and the black solid line represents the measured $\chi(z)$ at 56 K for comparison.

is within the expectation that all four $\chi(z)$ curves roughly follow the exponentially decaying feature. We thus extract the two signature parameters χ_0 and L_p from the reconstructed profiles, based on Eq. (1). The characteristic values are summarized in the inset table of Fig. 1(f). Second, the system shows monotonic behavior by decreasing the temperature, i.e., the helicity angle at the very top surface χ_0 becomes more divergent, while the surface twist penetration becomes shallower. It is worth noting that the surface twist penetration length varies from 50 to 9 nm by lowering the temperature suggesting a drastic change of the energetics from the system.

It thus motivates us to explore a possible reason that explains such sensitive temperature response of the 3D skyrmion structure. The most trivial reason for the temperature-dependent skyrmion behavior would come from the temperature-governed micromagnetic parameters, the exchange stiffness $J(T)$, the DMI strength $D(T)$, and the saturation magnetization $M_s(T)$. It is therefore reasonable to experimentally acquire these values at different temperatures for quantitative micromagnetic simulations, from which one is able to check whether the $\chi(z)$ modification is due to these aspects.

In order to obtain $M_s(T)$ of the single crystal Cu_2OSeO_3, we conducted magnetization measurements under the field of 170 mT and 30 mT by using superconducting quantum interference device (SQUID) magnetometer, as depicted in Fig. 2(a). To determine the other two crucial parameters Heisenberg exchange interaction $J(T)$ and the DMI strength $D(T)$, we employed ferromagnetic resonance (FMR) measurements in the conical state on the identical sample. It is established that $J(T)$ and $D(T)$ can be extracted via FMR under micromagnetic model. The static external magnetic field was applied perpendicular to the substrate, with $\mathbf{B} \parallel [100]$. The RF field component $\mathbf{h} \parallel [010]$ provided the necessary torque for excitation. The FMR spectra were recorded using a vector network analyzer, measuring the magnitude of the transmission parameter S_{12}, as shown in Fig. 2(b). The figure distinctly illustrates the presence of two conical modes $\pm Q$, which exhibit a clear decrease in resonance frequency and a reduction in spectral weight as the temperature increases.

The experimental knowledge about the $M_s(T)$ curve, together with the conical resonance spectra provide us sufficient information in order to extract the $J(T)$ and $D(T)$ parameters. We thus performed numerical fittings based on micromagnetic framework, targeting at the conical $+Q$ mode by using the atomistic spin model simulation software VAMPIRE [36]. The spin Hamiltonian can be written as

$$H = -\sum_{i \neq j} J_{ij}\mathbf{S}_i \cdot \mathbf{S}_j + \sum_{i \neq j} \mathbf{D}_{ij}^{\text{bulk}} \cdot (\mathbf{S}_i \times \mathbf{S}_j) - \sum_i \mu_s \mathbf{S}_i \cdot \mathbf{B}\,, \tag{8}$$

where J_{ij} and $\mathbf{D}_{ij}^{\text{bulk}}$ are the exchange interaction and the bulk DMI vector between atomic sites i and j, respectively. $\mathbf{S}_i$ and $\mathbf{S}_j$ are the unit vectors denoting the local classical spin. μ_s is the spin magnetization, and $\mathbf{B}$ is the external magnetic field. The simulation object was chosen to be a cubic cell with dimensions $a = b = c = 20$ Å. By fitting the dispersions of $+Q$ mode in Fig. 2(b), we obtain the values of D_{ij} and J_{ij} under varying temperatures, which are illustrated in Fig. 2(c). The simulation results, denoted by the red dots in Fig. 2(b), exhibit a remarkable agreement with the experimental data, thus substantiating the robustness of the parameters acquired from the simulation.

As we have successfully obtained these essential temperature-dependent parameters, we can now employ them in simulating the skyrmion system to predict the corresponding $\chi(z)$ values. As shown in Fig. 2(d), the simulated values of $\chi(z)$ at different temperatures exhibit almost identical profiles, which are, nevertheless, greatly deviating from the experimentally measured $\chi(z)$ evolution. Moreover, the simulated χ_0 is approximately double the magnitude of the experimental values, and the simulated L_p is considerably shorter than the experimental counterparts. We thus conclude that the temperature-governed micromagnetic parameters, i.e., M_S, J and D are not responsible for the temperature-dependent $\chi(z)$ profiles.

Therefore we are encouraged to explore additional, exotic energetic terms that can qualitatively explain the observed surface twist anomaly. It is demonstrated that an intermediate skyrmion structure, which falls between Néel and Bloch skyrmions, can be achieved through the interplay of bulk DMI (D^{bulk}) and interfacial DMI (D^{surf}) [37,38]. The helicity angle in such system is influenced by the ratio of $D^{\text{surf}}/D^{\text{bulk}}$ [39,40]. In noncentrosymmetric chiral magnets like Cu_2OSeO_3, translational symmetry are broken at both surface and bulk, leading to the emergence of a hybrid DMI that combines interfacial DMI (surface DMI) and bulk DMI.

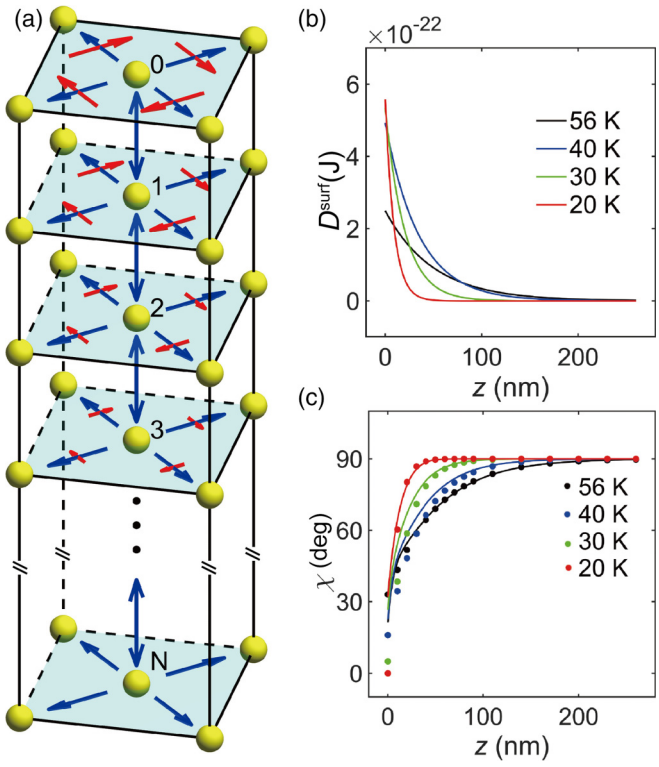

FIG. 3. (a) Schematic representation of hybrid DMI. Blue arrows and double arrows indicate intralayer and interlayer bulk DMI, respectively. Their directions depend on the atoms involved, determined by the antisymmetric nature of bulk DMI (e.g., when atom 0 interacts with atom 1, the arrow points downward; when atom 1 interacts with atom 0, the arrow points upward). Red arrows represent the surface DMI, and the arrow size reflects its exponential decay strength, with bulk DMI dominating at a distance from the surface. (b) Depth dependence of the simulated surface DMI strength at different temperatures. (c) $\chi(z)$ profiles at different temperatures. The colored dots represent some of the experimental data extracted from Fig. 1(f), while the solid lines correspond to the simulation results obtained after introducing the surface DMI shown in (b).

This hybrid DMI leads to skyrmions in the system exhibiting properties intermediate between Bloch-type and Néel-type, thereby affecting the helicity angle in the system. Based on these investigations, we believe that the introduction of an additional surface DMI alongside the bulk DMI is necessary to account for the phenomena we have observed.

Here we consider the hybrid DMI as $\mathbf{D}_{ij}^{\mathrm{hyb}} = \mathbf{D}_{ij}^{\mathrm{bulk}} + \mathbf{D}_{ij}^{\mathrm{surf}}$. It is reasonable to assume that the strength of bulk DMI remains uniform, while the strength of surface DMI exhibits an exponential decay from the surface to the bulk [41]. The surface DMI can be denoted as $|\mathbf{D}_{ij}^{\mathrm{surf}}| = D^{\mathrm{surf}} \exp(-z/L_{\mathrm{d}})$, where D^{surf} is the surface DMI strength, and L_{d} characterizes the decay rate of the surface DMI. Considering only nearest-neighbor interactions, all coupling terms between spins within a unit cell can be consolidated, as visualized in Fig. 3(a).

By applying the new model with the added surface DMI to fit the experimental data, we have obtained the values for D^{surf}. Figure 3(b) illustrates the depth dependence of D^{surf} at different temperatures. It is evident from the figure that at higher temperatures, the value of D^{surf} is more pronounced at the surface and exhibits a slower decay with depth, leading to a smaller L_{d}. Our simulations show that it is in good agreement with experimental results when $D^{\mathrm{surf}} = D^{\mathrm{bulk}}$ and $L_{\mathrm{d}} = L_{\mathrm{p}}$. Fig. 3(c) displays the $\chi(z)$ profile at different temperatures, calculated using the D^{surf} shown in Fig. 3(b). Notably, unlike the model that solely incorporates bulk DMI as observed previously [20], the model incorporating surface DMI fits the experimentally measured values effectively.

The observed temperature dependence behavior of surface DMI is reasonable, as the DMI typically decreases with temperature owing to thermal disorder. Specifically, at lower temperatures, the crystal lattice tends to be more stable and less affected by thermal fluctuations. This stability can lead to better-defined atomic arrangements and magnetic ordering at the surface, enhancing the surface DMI strength. Additionally, the electronic and spin configurations near the surface may become more ordered and aligned at lower temperatures. This alignment can enhance the DMI strength by promoting specific magnetic interactions that favor chiral spin structures. Furthermore, lower temperatures result in reduced thermal energy, leading to lower atomic and spin vibrations. This reduction in thermal disorder allows for more precise alignment of magnetic moments, leading to an increase in the surface DMI strength.

At this point, we have explored all the pivotal parameters that may have an impact on the surface twist effect. Our extensive investigation reveals that the introduction of surface DMI stands out as the primary determinant of the observed surface twist effect in Cu_2OSeO_3. The substantial magnitude of this interaction, nearly equivalent to bulk DMI, prompts a deeper inquiry into the underlying mechanism responsible for its existence.

Recent first-principles calculations indicated a strong interaction between ferroelectricity and ferromagnetism in multiferroic heterostructures like $BaTiO_3/SrRuO_3$ and $BiFeO_3/BaTiO_3$ [42,43]. For instance, the DMI at the interface can be enhanced by ferroelectric polarization. Considering that Cu_2OSeO_3 is a typical ferroelectric material that hosts skyrmions, it is reasonable to expect that these phenomena could manifest within this specific context.

The primary mechanism for magnetoelectric coupling in insulating Cu_2OSeO_3 is the $d-p$ hybridization model, which emerges from the interaction between O^{2-} and Cu^{2+}. This model entails the modulation of covalency between metal d and ligand p orbitals, influenced by the local magnetization direction via spin-orbit interaction. Consequently, a local electric dipole is generated along the bond direction within this framework. Therefore each magnetic skyrmion can induce spatially varying local electric charge distributions owing to relativistic spin-orbit interactions [44,45]. Based on the relative orientation between the magnetic field and the crystallographic direction, a spatially varying electric charge density distribution $\rho(\mathbf{r}) = -\nabla \cdot \mathbf{p}(\mathbf{r})$ is expected. The local electric polarization relates to the local magnetization density distribution via $\mathbf{p} \propto (m_y m_z, m_z m_x, m_x m_y)$ [44,46,47].

Using the equations mentioned above, we have calculated the local electric charge density distribution in real space for individual skyrmion strings within Cu_2OSeO_3. Figures 4(a)–4(d) present the local electric charge density distribution in the x-y plane for the topmost layer of a skyrmion at different

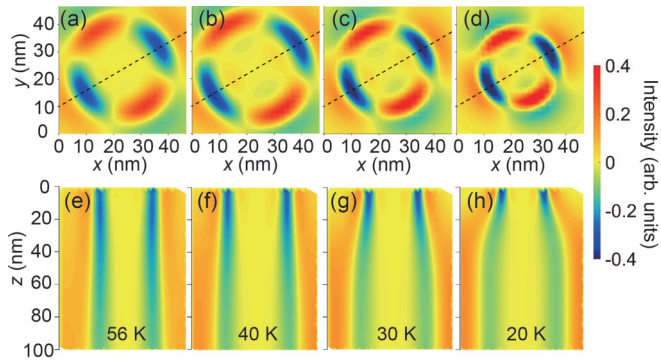

FIG. 4. Calculated spatial distributions of (a)–(d) the local electric charge ρ for the skyrmion of the most top surface ($z = 0$ nm) and (e)–(h) the corresponding depth-dependence vertical cross section through the dotted line of (a)–(d). The background color represents the relative value of ρ.

temperatures, while Figs. 4(e)–4(h) represent the corresponding distribution along the z direction. These figures show that as the temperature decreases, the skyrmion diameter reduces, and the local electric charge density ρ progressively contracts towards the center of the skyrmion. Furthermore, the local electric charge density near the surface ($z = 0$) increases, indicating an inclination to accumulate at the surface. The variation in polarized charge density concerning both temperature and depth aligns with the behavior of $\chi(z)$, providing compelling evidence for the likely role of ferroelectric polarization in the existence of surface DMI.

In summary, the temperature-dependent CD-REXS experiments have demonstrated that this surface twist effect exhibits a dynamic response to temperature changes. To model and analyze this behavior, we firstly performed micromagnetic simulations using the standard surface twist model, taking into account all the temperature-varying parameters. Surprisingly, this model failed to capture the observed temperature-dependent surface twist behavior. On the other hand, the agreement dramatically improved when an additional surface DMI term is introduced. Such surface DMI has an unexpected amplitude that are even comparable with the bulk DMI value. Furthermore, we delved into the distribution of polarization charge density on the surface of Cu_2OSeO_3 and its relation to the magnetic structure concerning both temperature and depth. The observations of charge density clustering near the surface were highly consistent with the variations in $\chi(z)$ and provided compelling evidence for the involvement of ferroelectric polarization in driving the surface DMI. Our research unravels the complex connection between surface effects, ferroelectric polarization, and the formation of magnetic skyrmions. These findings not only contribute to the fundamental understanding of magnetic skyrmions but also open up exciting prospects for engineering and tailoring skyrmionic devices with improved control and functionality.

The resonant soft x-ray scattering experiments were carried out on the RASOR diffractometer at beamline I10 at the Diamond Light Source (Didcot, UK) under Proposal No. MM30645-1. This work was supported by the National Key R&D Program of China under Contract No. 2022YFA1403600 and No. 2020YFA0309400, the science and Technology Commission of the Shanghai Municipality (21JC1405100), the National Natural Science Foundation of China (Grant No. 12074257), and the Double First-Class Initiative Fund of ShanghaiTech University. K.J.R. acknowledges the support from the National Natural Science Foundation of China with Grants No. 12004249 and No. 12374162).

[1] A. N. Bogdanov and D. A. Yablonskii, Zh. Eksp. Teor. Fiz. **95**, 178 (1989) [Sov. Phys. JETP **68**, 101 (1989)].
[2] N. Nagaosa and Y. Tokura, Nat. Nanotechnol. **8**, 899 (2013).
[3] A. Neubauer, C. Pfleiderer, B. Binz, A. Rosch, R. Ritz, P. G. Niklowitz, and P. Böni, Phys. Rev. Lett. **102**, 186602 (2009).
[4] F. Jonietz, S. Mühlbauer, C. Pfleiderer, A. Neubauer, W. Münzer, A. Bauer, T. Adams, R. Georgii, P. Böni, R. A. Duine, K. Everschor, M. Garst, and A. Rosch, Science **330**, 1648 (2010).
[5] T. Schulz, R. Ritz, A. Bauer, M. Halder, M. Wagner, C. Franz, C. Pfleiderer, K. Everschor, M. Garst, and A. Rosch, Nat. Phys. **8**, 301 (2012).
[6] J. Sampaio, V. Cros, S. Rohart, A. Thiaville, and A. Fert, Nat. Nanotechnol. **8**, 839 (2013).
[7] J. Iwasaki, M. Mochizuki, and N. Nagaosa, Nat. Nanotechnol. **8**, 742 (2013).
[8] W. Jiang, P. Upadhyaya, W. Zhang, G. Yu, M. B. Jungfleisch, F. Y. Fradin, J. E. Pearson, Y. Tserkovnyak, K. L. Wang, O. Heinonen, S. G. E. te Velthuis, and A. Hoffmann, Science **349**, 283 (2015).
[9] M. Mochizuki, Phys. Rev. Lett. **108**, 017601 (2012).
[10] Y. Onose, Y. Okamura, S. Seki, S. Ishiwata, and Y. Tokura, Phys. Rev. Lett. **109**, 037603 (2012).
[11] T. Schwarze, J. Waizner, M. Garst, A. Bauer, I. Stasinopoulos, H. Berger, C. Pfleiderer, and D. Grundler, Nat. Mater. **14**, 478 (2015).
[12] N. Nagaosa and Y. Tokura, Phys. Scr. **T146**, 014020 (2012).
[13] X. Z. Yu, N. Kanazawa, W. Z. Zhang, T. Nagai, T. Hara, K. Kimoto, Y. Matsui, Y. Onose, and Y. Tokura, Nat. Commun. **3**, 988 (2012).
[14] S. Woo, K. Litzius, B. Krüger, M.-Y. Im, L. Caretta, K. Richter, M. Mann, A. Krone, R. M. Reeve, M. Weigand, P. Agrawal, I. Lemesh, M.-A. Mawass, P. Fischer, M. Kläui, and G. S. D. Beach, Nat. Mater. **15**, 501 (2016).
[15] A. Crépieux and C. Lacroix, J. Magn. Magn. Mater. **182**, 341 (1998).
[16] Y. Tokura and N. Kanazawa, Chem. Rev. **121**, 2857 (2021).
[17] S. L. Zhang, G. van der Laan, W. W. Wang, A. A. Haghighirad, and T. Hesjedal, Phys. Rev. Lett. **120**, 227202 (2018).
[18] X. Z. Yu, Y. Onose, N. Kanazawa, J. H. Park, J. H. Han, Y. Matsui, N. Nagaosa, and Y. Tokura, Nature (London) **465**, 901 (2010).
[19] S. Heinze, K. von Bergmann, M. Menzel, J. Brede, A. Kubetzka, R. Wiesendanger, G. Bihlmayer, and S. Blügel, Nat. Phys. **7**, 713 (2011).

[20] S. Zhang, G. van der Laan, J. Müller, L. Heinen, M. Garst, A. Bauer, H. Berger, C. Pfleiderer, and T. Hesjedal, Proc. Natl. Acad. Sci. USA **115**, 6386 (2018).
[21] S. A. Meynell, M. N. Wilson, H. Fritzsche, A. N. Bogdanov, and T. L. Monchesky, Phys. Rev. B **90**, 014406 (2014).
[22] A. O. Leonov, Y. Togawa, T. L. Monchesky, A. N. Bogdanov, J. Kishine, Y. Kousaka, M. Miyagawa, T. Koyama, J. Akimitsu, T. Koyama, K. Harada, S. Mori, D. McGrouther, R. Lamb, M. Krajnak, S. McVitie, R. L. Stamps, and K. Inoue, Phys. Rev. Lett. **117**, 087202 (2016).
[23] F. N. Rybakov, A. B. Borisov, S. Blügel, and N. S. Kiselev, New J. Phys. **18**, 045002 (2016).
[24] D. McGrouther, R. J. Lamb, M. Krajnak, S. McFadzean, S. McVitie, R. L. Stamps, A. O. Leonov, A. N. Bogdanov, and Y. Togawa, New J. Phys. **18**, 095004 (2016).
[25] K. Ran, Y. Liu, H. Jin, Y. Shangguan, Y. Guang, J. Wen, G. Yu, G. van der Laan, T. Hesjedal, and S. Zhang, Nano Lett. **22**, 3737 (2022).
[26] H. Jin, W. Tan, Y. Liu, K. Ran, R. Fan, Y. Shangguan, Y. Guang, G. van der Laan, T. Hesjedal, J. Wen, G. Yu, and S. Zhang, Nano Lett. **23**, 5164 (2023).
[27] F. N. Rybakov, A. B. Borisov, and A. N. Bogdanov, Phys. Rev. B **87**, 094424 (2013).
[28] G. van der Laan, S. Zhang, and T. Hesjedal, AIP Adv. **11**, 015108 (2021).
[29] S. Seki, X. Z. Yu, S. Ishiwata, and Y. Tokura, Science **336**, 198 (2012).
[30] S. L. Zhang, A. Bauer, D. M. Burn, P. Milde, E. Neuber, L. M. Eng, H. Berger, C. Pfleiderer, G. van der Laan, and T. Hesjedal, Nano Lett. **16**, 3285 (2016).
[31] K. Ran, Y. Liu, Y. Guang, D. M. Burn, G. van der Laan, T. Hesjedal, H. Du, G. Yu, and S. Zhang, Phys. Rev. Lett. **126**, 017204 (2021).
[32] A. Chacon, L. Heinen, M. Halder, A. Bauer, W. Simeth, S. Mühlbauer, H. Berger, M. Garst, A. Rosch, and C. Pfleiderer, Nat. Phys. **14**, 936 (2018).
[33] L. J. Bannenberg, H. Wilhelm, R. Cubitt, A. Labh, M. P. Schmidt, E. Lelièvre-Berna, C. Pappas, M. Mostovoy, and A. O. Leonov, npj Quantum Mater. **4**, 11 (2019).
[34] See Supplemental Material at http://link.aps.org/supplemental/10.1103/PhysRevB.109.L220402 for resonant elastic x-ray scattering measurements, providing details of the experimental setup, the data acquisition, and the data processing, as well as micromagnetic simulation details, and a list of the crucial magnetic interaction parameters used in simulation.
[35] S. L. Zhang, *Chiral and Topological Nature of Magnetic Skyrmions* (Springer, 2018).
[36] R. F. Evans, W. J. Fan, P. Chureemart, T. A. Ostler, M. O. Ellis, and R. W. Chantrell, J. Phys.: Condens. Matter **26**, 103202 (2014).
[37] W. Li, I. Bykova, S. Zhang, G. Yu, R. Tomasello, M. Carpentieri, Y. Liu, Y. Guang, J. Gräfe, M. Weigand *et al.*, Adv. Mater. **31**, 1807683 (2019).
[38] W. L. N. C. Liyanage, N. Tang, L. Quigley, J. A. Borchers, A. J. Grutter, B. B. Maranville, S. K. Sinha, N. Reyren, S. A. Montoya, E. E. Fullerton, L. DeBeer-Schmitt, and D. A. Gilbert, Phys. Rev. B **107**, 184412 (2023).
[39] K.-W. Kim, K.-W. Moon, N. Kerber, J. Nothhelfer, and K. Everschor-Sitte, Phys. Rev. B **97**, 224427 (2018).
[40] H. Vakili, Y. Xie, and A. W. Ghosh, Phys. Rev. B **102**, 174420 (2020).
[41] X. Xie, K. Ran, Y. Liu, R. Fan, W. Tan, H. Jin, M. Valvidares, N. Jaouen, H. Du, G. van der Laan, T. Hesjedal, and S. Zhang, Phys. Rev. B **107**, L060405 (2023).
[42] L. Wang, Q. Feng, Y. Kim, R. Kim, K. H. Lee, S. D. Pollard, Y. J. Shin, H. Zhou, W. Peng, and D. Lee, Nat. Mater. **17**, 1087 (2018).
[43] W. Wang, W. Sun, G. Zhang, F. Ren, Y. Wang, C. You, and Z. Cheng, J. Adv. Res. **24**, 371 (2020).
[44] S. Seki, S. Ishiwata, and Y. Tokura, Phys. Rev. B **86**, 060403(R) (2012).
[45] J. H. Yang, Z. L. Li, X. Z. Lu, M.-H. Whangbo, S.-H. Wei, X. G. Gong, and H. J. Xiang, Phys. Rev. Lett. **109**, 107203 (2012).
[46] H. Murakawa, Y. Onose, S. Miyahara, N. Furukawa, and Y. Tokura, Phys. Rev. B **85**, 174106 (2012).
[47] S. Seki and M. Mochizuki, *Skyrmions in Magnetic Materials* (Springer, 2016).